Chromatin-modifying enzymes as modulators of nuclear size during lineage differentiation

Lingjun Meng[1,*], Evgeny Zatulovskiy[2], Yohei Shibuya[1], Katie Marie Schaukowitch[1], Gernot Neumayer[1], Jan M. Skotheim[2], Marius Wernig[1].

[1]Institute for Stem Cell Biology and Regenerative Medicine, Department of Pathology, Stanford University, CA 94305, USA

[2]Department of Biology, Stanford University, Stanford, CA 94305, USA.

*Correspondence: lingjun@stanford.edu, menglingjundl@gmail.com

Key word: histone demethylases, nuclear size, differentiation, cancer.

Abstract

The mechanism of cell size determination and alteration during normal lineage development and cancer pathologies which is not fully understood. As recently reported, chromatin modification can change nuclear morphology. Therefore, we screened a range of pharmacological chemical compounds that impact the activity of chromatin-modifying enzymes, in order to get a clue of the specific types of chromatin-modifying enzymes that remarkably effect nuclear shape. We used three assays to measure the nuclear size and cell size. The novel coulter counter was presented here and validated with using flow cytometry and confocal fluorescence microscopy to measure size. We found that interrupted activity of chromatin-modifying enzymes is associated with nuclear

shape abnormalities. Furthermore, the activity of chromatin-modifying enzymes perturbs cell fate determination in cellular maintenance and lineage commitment. Our results present a new idea in understanding the relation of chromatin-modifying enzymes and nuclear size during lineage differentiation.

Introduction

As reported, nuclear volume is an important morphological parameter that can change during cancer progression [1]. After confocal microscopy was discovered and broadly used to observe the detailed structure of specific objects within the cell, the most fascinated cellular organelle - nucleus was researched more carefully. Recent studies have also highlighted that nuclear shape can influence fate decisions [2]. Embryonic stem cells (ESCs) differentiation is accompanied by an increase in chromatin condensation [3] leading to an increase in nuclear stiffness [4] and a decrease in nuclear size. As known, the nuclear size of stem cells is extremely bigger than terminal differentiated cells. Cell differentiation is corresponding with chromatin marks reset, which raises the question of whether chromatin's contribution to nuclear mechanics affects nuclear morphology as well as cell fate. It is therefore critical to identify the contributions of various chromatin-modifying enzymes that are relevant to cell fate decisions, and consequently display nuclear size alteration.

While previous studies have focused on utilizing microscopy examination to achieve the visualization of nucleus via its two-dimensional structure, here we employed two novel assays,

41 such as flow cytometry [5,6] and coulter counter [7] to measure the nuclear and cell size via three-
42 dimensional structure. We used flow cytometry to measure forward scatter (FSC) of individual
43 cells [8], cell volume was identified by forward scatter area (FSC-A), and nuclear volume was
44 identified by Hoechst-W (width) after staining with Hoechst. By using coulter counter, cells flow
45 through a measurement chamber where they displace an isotonic solution to cause a volume-
46 proportional change in electrical impedance [7]. Coulter counter measures cell number and size in
47 high throughput as well as flow cytometry. The high throughput quantitative analysis of 3D nuclear
48 architecture facilitates better investigation of a great variability of nuclear shapes, in order to fully
49 understand the nuclear contour related cell fate decisions also including cancer cell fate decisions.
50 Nuclear architecture is impacted via chromosome structure which is determined by histone
51 modifications. The cellular differentiation from stem cells to differentiated cells which is
52 corresponding with nuclear size reduction as well as chromosome condense. Histone demethylases
53 have also been reported to be critical enzymes that regulate the balance between self-renewal and
54 differentiation in hESCs (human embryonic stem cells) [9-12]. Accordingly, we broadly utilized
55 chromatin-modifying enzymes inhibitors to treat stem cells such as hESCs, NPCs (neural
56 progenitor cells), and later a cancer cell line such as leukemia cells. We demonstrated that the
57 irregularities of nuclear contour were highly related to pharmacological inhibition of chromatin-
58 modifying enzyme activity. As known, upregulation or downregulation of histone demethylases is
59 observed in various types of cancer and is associated with higher rates of malignancy and relapse
60 after treatment [13]. In particular, GASC1 (gene amplified in squamous cell carcinoma, also known

61 as KDM4C, a histone demethylase) promotes chromosomal instability and transcription initiation,
62 therefore, plays a causative role in cancer cells driven by its dysregulation [14]. GASC1 was found
63 aberrant expression in esophageal squamous carcinomas [15], medulloblastomas [16], glioma [17], breast
64 cancer [18], and prostate cancer [19]. In addition, GASC1 plays an essential role in the transition of
65 mouse ESCs (mESCs) to endothelial cells [20]. Consistently, we demonstrated that upregulation of
66 GASC1 impairs the differentiation of undifferentiated hESCs to terminal differentiated neural cells.
67 Moreover, upregulation of GASC1 impairs the proliferation of leukemia cells due to cell cycle
68 arrest in the G0/G1 phase and indicated misshapen nucleus. Taken together, epigenetic
69 perturbations are likely to be the cause for misregulation of nuclear size and of certain cancer cell
70 fates [21].
71
72 **Result**
73 **The nuclear size is associated with cell fate decision and chromatin-modifying enzyme**
74 **activity**
75 Size and shape are distinctive aspects of nuclear structure. Nuclear size impacts cell function,
76 and is altered according to the specific status of cell types during cell development [22]. It is unclear
77 which modulators effect the altered nuclear size during cell fate transformation. To investigate the
78 distinct nuclear size of various cell types, we employed highly efficient differentiation methods to
79 interrogate the size change of nucleus during lineage differentiation. To differentiate NPCs from
80 hESCs, we used two molecular compounds, SB431542 and LDN193189, to inhibit the TGF-β

81 (transforming growth factor beta) and BMP (bone morphogenetic protein) pathways, which are
82 also called Dual SMAD inhibitors [22,23]. In addition, as we previously used, overexpression of Ngn2
83 (neuronal gene neurogenin-2) could converts hESCs into iN cells (induced neuronal cells) with
84 nearly 100% yield in less than two weeks. The hESCs-derived iN cells grow long axon that conduct
85 electrical impulses away from the neuron's cell body [24]. We utilized 300 nM DAPI to stain hESCs,
86 hESC-derived NPCs, hESC-derived iN cells for 5 min, then examining the dynamic change of the
87 nuclear size via measuring the area of nucleus under a fluorescence microscope (Fig. 1a).
88 Fluorescence images of nucleus stained with DAPI were acquired through imaging at 40×
89 resolution. Notably, it was shown that there is a reduced size of approximately 40% from hESCs
90 to NPCs, and 24% decrease from NPCs to iN cells (Fig. 1b). Consistently as reported, the nuclear
91 size of hESCs is bigger than NPCs, and the nuclear size of NPCs is bigger than iN cells. In addition,
92 it was shown that the nuclear size of hESCs and NPCs are in a wider range than iN cells, which
93 indicates that there is a potential of stem cells in nuclear dynamics. The different sizes of nuclei
94 may correspond with hESCs, NPCs, and neural cells characterized with distinct unique chromatin
95 architecture. During the reprogramming of cell identity and cell fate determination,
96 heterochromatin plays a critical role. H3K9me3 (Tri-methylation of histone H3 lysine 9) is a
97 histone mark associated with heterochromatin, has emerged as a key player in repressing lineage-
98 inappropriate genes, and shielding them from activation by transcription factors. We investigated
99 the H3K9me3 expression in hESCs and hESC-derived NPCs by immunofluorescence staining. It
100 was shown that there are high levels of expression of H3K9me3 in the nucleus (Fig. 1c). To directly

101 address the role of chromatin in nuclear morphology, we employed a range of commercially
102 available chemical compound inhibitors of the enzymes that modulate histone modification state
103 to manipulate chromatin alterations to treat hESCs and hESC-derived NPCs (Fig. 1d, e). These
104 available inhibitors of chromatin-modifying enzymes that were represented the various functions
105 of chromatin regulation, which helped us to investigate broadly to chromatin-modifying enzymes
106 associated with nuclear alteration. We purchased these inhibitors from tocris as method shown. As
107 reported, GSK-J1 is a highly potent inhibitor of the H3K27 histone demethylases JMJD3 (KDM6B)
108 and UTX (KDM6A), likewise inhibits KDM5B, KDM5C, and KDM5A to increase H3K27me3.
109 Histone demethylases inhibitor increased heterochromatin levels and chromatin-based nuclear
110 stiffness. Heterochromatin is highly condensed DNA that leads to gene silencing [25]. R2-HG is
111 oncometabolite produced by mutant isocitrate dehydrogenase 1 (IDH1) and IDH2, inhibits
112 KDM4A in murine embryonic fibroblasts as well as increases H3K9me3, H3K36me3. 5-Aza is a
113 DNA methyltransferase inhibitor that induces demethylation. GSK-LSD1 is a potent and selective
114 lysine specific demethylase 1 (LSD1) inhibitor, increasing H3K4me3, H3K9me3, H3K27me3.
115 IOX1 is a histone demethylase JMJD inhibitor, increasing H3K36me3, H3K9me3, H3K27me3.
116 JIB04 is a pan Jumonji histone demethylase inhibitor that inhibits H3K4 demethylases, decreases
117 H3K36me3, H3K9me3. NSC636819 is a KDM4A/KDM4B inhibitor, increasing H3K9me3. PBIT
118 is a JARID1 (Jumonji AT-Rich Interactive Domain 1) inhibitor that increases H3K4me3. C646 is
119 a inhibit histone acetyltransferase, which corresponds predominantly to decompacted euchromatin,
120 allowing transcription factors to bind to regulatory sites on DNA, in order to cause transcriptional

121 activation [26]. Through the treatment with compounds function as chromatin-modifying enzyme
122 inhibitors, we found that 5-Aza treatment enlarges the nuclear size of both hESCs and hESC-
123 derived NPCs remarkably (Fig. 1d, e), also some other inhibitors. In contrast, 5-Aza treatment
124 slightly reduced the nuclear size of hESC-derived iN cells (Fig. 1f). The great increase in nuclear
125 size of hESCs from 5-Aza treatment that indicated that modulation of chromatin-modifying
126 enzymes is enabled to change nuclear size (Fig. 1g). It suggested that perturbation of chromatin-
127 modifying enzyme activity alters nuclear size in normal cells.
128
129 **Inhibition of chromatin-modifying enzyme enlarges hESCs nuclear size**
130 To investigate the nuclear size and cell size in various methods, we employed flow cytometry
131 and coulter counter to measure the nuclear size and cell size, then compared with confocal
132 fluorescence microscopy by DAPI staining used above. Flow cytometry optical scatter was used
133 to measure the size of live cells. This parameter is a measurement of the amount of the laser beam
134 that passes around the cell. This gives a relative size for the cell. Therefore, the forward scatter
135 area (FSC-A) parameter was used as a readout for cell size. Hoechst 33342 is a dye that binds to
136 AT-rich sequences of double-stranded DNA. So, we used Hoechst-W (width) indicates the nuclear
137 size (Fig. 2a, b, c). From the flow cytometric size measurements of hESCs after inhibitors
138 treatment for 7 days, which was shown that cell size distributions of hESCs were affected by these
139 chromatin-modifying enzymes inhibitors, especially in 5-Aza and IOX1 treatment compared to
140 DMSO control (Fig. 2d, e). The nuclear size indicated by Hoechst-W was increased 13% in 5-Aza

141 treatment, and the cell size indicated by FSC-A was increased 20%, which suggested the major
142 contributor to cell size change is the nucleus. As above shown, we also measured the nucleus size
143 of hESCs by DAPI staining after inhibitors treatment for 7 days (Fig. 1d). It was shown that 5-Aza
144 significantly enhances the nuclear size of hESCs (Fig. 1d). Treating with high concentrations of
145 IOX1 which revealed the cytotoxic effects on hESCs. Therefore, we tested a series of
146 concentrations of compounds for hESCs treatment. The high concentrations of inhibitors caused
147 cell death of hESCs, such as 100 mM GSK-J1, 100 mM IOX1, 1 mM JIB04, 10 mM PBIT, 25 mM
148 C646, especially, 10 μM, 1 mM, 10 mM 5-Aza induced numerous of hESCs death. The high
149 concentrations of inhibitors have cytotoxic effects on cells and impact cells alive. However, hESCs
150 grow well in 60 μM, 1 mM, 10 mM GSK-J1, 100 mM R2HG, 10 mM and 100 mM GSK-LSD1,
151 1 mM and 10 mM IOX1, 10 μM and 100 μM JIB04, 10 μM and 10 mM NSC636819, 100 μM and
152 1 mM PBIT, 250 μM and 2.5 mM C646 treatment. Furthermore, we performed coulter counter
153 analysis to measure the corresponding cell volume of hESCs in a dynamics pattern after inhibitors
154 treatment for 6 days. Coulter counter is an apparatus for counting and sizing particles suspended
155 in electrolytes, which provides a relative estimate of the regularity of each nucleus. After broadly
156 measuring the volume of each cell with treatment, it demonstrated that cellular volume of hESCs
157 measured as FL (Femtoliter) was increased in 5-Aza and IOX1 treatment compared with DMSO
158 control, which was consistent with flow cytometry measurement (Fig. 2f). The three different
159 assays were all indicated that compounds function as chromatin-modifying enzyme inhibitors
160 which effect nuclear size alteration, possibly through modulating histone dynamics. It had been

161 shown that utilizing histone methyltransferase inhibitors to decrease heterochromatin results in a
162 softer nucleus and nuclear blebbing, without perturbing lamins. Histone demethylase inhibitors
163 increase heterochromatin and chromatin nuclear rigidity [27]. Given that measurements in these
164 reports demonstrate that there is evidence that nuclear size abnormalities can be caused by
165 alterations to chromatin regulatory proteins.
166

167 **Inhibition of chromatin-modifying enzyme effects nuclear size and cell identification of NPCs**

168 To gain further insights into whether these inhibitors not only impact cell death also effect
169 additional features, such as cell fate decisions, we treated the hESC-derived NPCs with DMSO, 5-
170 Aza, IOX1, JIB04, and PBIT. The concentration we used that was tested and same concentration
171 was used as hESCs treatment. Then imaged hESC-derived NPCs after staining for Sox1 (green),
172 PI (red), and DAPI (blue) (Fig. 3a). As known, Sox1 is a neural stem cell marker. It was observed
173 that the expression of Sox1 was significantly reduced in a large number of NPCs in 5-Aza, JIB04,
174 and PBIT treatment. To eliminate the possibility of Sox1 expression decrease caused by cell death,
175 we performed propidium iodide (PI) staining to NPCs after inhibitors treatment. As known, PI is
176 not permanent to live cells but is used to detect dead cells in a population. It was shown that Sox1
177 silence was not caused by cell death due to PI staining being negative. Except only IOX1 increased
178 PI staining in NPCs which suggested that 10 mM IOX1 treatment induces cytotoxic responses of
179 NPCs occur as a consequence of cell death. It suggested that the compound inhibitors of chromatin-
180 modifying enzymes perturb cell identification. We also measured the cell size of hESC-derived

181 NPCs by the coulter counter after inhibitors treatment for 9 days (Fig. 3b). The treatment of 5-Aza,
182 GSK-LSD1, IOX1, and JIB04 enhanced the nuclear size of NPCs. Collectively, inhibition of
183 chromatin-modifying enzymes activity enabled to impact nuclear size in both hESCs and NPCs
184 which consequently leads cell fate to aberrant states.
185
186 **Inhibition of chromatin-modifying enzyme effects leukemia cell nuclear architecture**
187 As above discussed, chromatin-modifying enzyme activity is highly associated with nuclear
188 size alteration in normal stem cells during lineage differentiation. As reported, cancer cells are
189 known to develop larger nuclei as they become more malignant and increase the nuclear-to-
190 cytoplasmic ratio [28]. The mechanisms that underlie the increase in nuclear size in malignant cells
191 remain largely unknown. Abnormal nuclear morphology has been used for cancer diagnoses for
192 nearly a century in tests such as the Pap smear [29]. The novel assay for detecting nuclear shape
193 alteration of 3D structure is helpful to better understand. Therefore, we utilized flow cytometric
194 size measurements to measure the nuclear size of K562 leukemia cells, in order to investigate the
195 distinctive features of chromatin-modifying enzyme activity in cancer cells compared to normal
196 stem cells. We performed flow cytometry to measure the nuclear size and cell size of K562
197 leukemia cells after compound inhibitors treatment for 5 days (Fig. 4a, b, c). We tested a series of
198 concentrations of compound inhibitors for K562 cells treatment. Consistent with hESCs, high
199 concentrations of inhibitors caused cell death of K562 cells. Especially, high dose and long-time
200 of 5-Aza and PBIT treatment induce cell death. In addition, we photographed the DAPI stained

201 nucleus of K562 cells treated with DMSO as control and 5-Aza, IOX1, GSK-LSD1, and JIB04. It
202 was shown that K562 cells treated with inhibitors have a bigger size of nucleus and twisted shape
203 as clover, especially in IOX1, GSK-LSD1, and JIB04 treatment (Fig. 4d). It demonstrated that
204 there is the irregularity of nuclear contour in inhibitors treatment from the visible fluorescent
205 images. The most studied types of nuclear morphological abnormalities are protrusions from the
206 normally ellipsoidal nucleus, termed "blebs." K562 cells showed a "blebs" shape and seem prefer
207 to have a twisted nuclear shape but not die as quickly as hESCs and NPCs did. We measured the
208 nuclear size by DAPI staining after K562 cells were treated with inhibitors, it was shown that the
209 increased percentage of nuclear size of K562 cells is 5% ~ 44% in inhibitors treatment compared
210 to DMSO control, especially higher in 5-Aza and IOX1 treatment (Fig. 4e). It all suggested that
211 not only nuclear size change but also nucleus misshapen are indicated the pathological change of
212 K562 leukemia cells induced by inhibition of chromatin-modifying enzymes activity. Furthermore,
213 to measure nuclear size and cell size of cancer cells in 3D, we utilized flow cytometry, coulter
214 counter, and DAPI staining to measure the nuclear size and cell size of K562 leukemia cells. The
215 size of cancer cells was more similar to hESCs but bigger than NPCs (Fig. 4f). After inhibitors
216 treatment for 7 days (10 μM GSK-J1, 100 μM R2HG, 1 μM 5-Aza, 10 μM GSK-LSD1, 10 μM
217 IOX1, 100 μM JIB04, 10 μM NSC636819, 1 μM PBIT, 2.5 μM C646), compared to DMSO control,
218 treatment of 5-Aza and IOX1 markedly lead to the enlargement of the nuclear size and cell size of
219 K562 leukemia cells (Fig. 4f). Comparing these quantitative approaches, which we validated with
220 measurement by confocal microscopy, it reveals that all assays support chromatin-modifying

221 enzyme activity directly effects nuclear size. Except for lamina perturbation affecting nuclear
222 abnormalities [30], it also suggested that enlarged and twisted nuclear size effect the survival of K562
223 cells which is associated with chromatin-modifying enzyme activity.
224
225 **Upregulated GASC1 impairs differentiation from hESCs to iN cells**
226 As we previously discussed, the nuclear size dramatically reduced from hESCs to NPCs, and
227 to iN cells during lineage differentiation. Additionally, we want to validate the specificity of the
228 targeted chromatin-modifying enzyme instead of using chemical compounds. So, we selected three
229 represented histone enzymes such as GASC1, DNMT3A, and KDM4A, based on the screening of
230 inhibitors of chromatin-modifying enzyme activity, to investigate the impact of chromatin-
231 modifying enzymes in lineage differentiation. GASC1 (lysine-specific demethylase 4C, KDM4C)
232 is a histone demethylase as well as KDM4A (lysine-specific demethylase 4A), they both belong to
233 the families of lysine demethylases (KDM). DNMT3A (DNA methyltransferase 3A) catalyzes 5-
234 methylcytosine methylation. 5-Aza inhibits DNA methyltransferase (DNMT). We used the
235 doxycycline (dox)-inducible lentiviral vector system to transduce empty vector plasmid as control
236 and GASC1, DNMT3A, KDM4A into the hESCs H1 cell line, separately. As mentioned above,
237 we used the same approach to induce neuronal cells from differentiating hESCs by Ngn2
238 overexpression [24]. It was shown that there is a significantly high efficiency of wt hESCs
239 differentiating to iN cells as nearly 100%. The iN cells display a mature neural morphology with
240 axon extension and packaged smaller cell nucleus (Fig. 5a). We stained hESC-iN cells with a

241 neuronal marker Tuj1 (tubulin beta-III) and a pluripotent marker Sox2, it demonstrated that iN
242 cells differentiated from wt hESCs showed Tuj1 positive expression and long axon extension, no
243 Sox2 indicated hESCs left, which also occurred in KDM4A overexpressed hESC-iN cells. In
244 contrast, hESC-iN cells with induced overexpression of GASC1 and DNMT3A that grew few
245 extend axons. In addition, a large number of cells were Sox2 positive during differentiation (Fig.
246 5a). After measurement analysis of neurite length at 14 days of iN cell differentiation, we found
247 that hESC-iN cells with GASC1 and DNMT3A overexpression grew remarkably shorter neurite
248 compared to wt and KDM4A overexpressed iN cells (Fig. 5b). Perturbation of chromatin-
249 modifying enzymes activity alters the molecular and cellular identity of stem cells. Overall, these
250 data suggested that chromatin-modifying enzymes can drive lineage specification as well as assist
251 nuclear reconstruction, in order to facilitate a smoother transition from stem cells to differentiated
252 cells.
253
254 **GASC1 promotes aberrant nuclear structure and cell cycle arrest of leukemia cells**
255 As mentioned above, these chromatin-modifying enzymes effect lineage differentiation of
256 hESCs. These hESC-iN cells with GASC1 and DNMT3A aberrant expression retain their
257 proliferation capability, fail differentiation, and acquire resistance to cell death. As previously
258 reported, IDH1 mutated cells generate R(2)-2-hydroxyglutarate (2HG) [31], which causes GASC1
259 mediated hypermethylation [19,32]. IDH1 gene mutations occur frequently in AML (acute
260 lymphoblastic leukemia). Accordingly, we investigated the role of GASC1 in K562 leukemia cells

261 differentiation. Basically, healthy and as cultured K562 cells are spherical in shape without any
262 structural irregularities and distortions, and grow in suspension (Fig. 6a). After being differentiated
263 by Ngn2 overexpression for 14 days, it was shown that a portion of K562 cells grew spike, and
264 Tuj1 was not abundantly expressed (Fig. 6a). K562 cells are hard to differentiate. When adding
265 dox in cell culture for inducing GASC1 overexpression, the majority of K562 leukemia cells began
266 to change their morphology from smooth surfaces of spherical shape to twisted cellular shape
267 compared with no dox-induced K562 cells (Fig. 6b, c). The abnormal nuclear morphology and
268 protrusions termed "blebs" are both associated with chromatin alterations [27]. To validate the cell
269 shape change corresponding to nucleus change, we stain K562 cells with DAPI. Under microscope
270 examination of GASC1 overexpressed K562 cells with or without dox, we found that it is
271 consistent with cell shape change in dox-induced overexpressed K562 cells, that showed nucleus
272 enlarges and shapes as clover (Fig. 6d, e). To investigate the twisted shape consequently provides
273 benefits of growth of the K562 cells or not, we employed the Brdu cell proliferation assay to
274 interrogate the cell cycle of K562 cells growth. The dox-induced K562-GASC1 cells significantly
275 proliferate slower than the no dox-induced K562-GASC1 cells (Fig. 6f, g). Meanwhile, we count
276 the cell number of K562 cells with or without dox-induced GASC1 overexpression, it reveals that
277 there is a significant reduction in the growth of K562 cells with GASC1 overexpression (Fig. 6h).
278 To explore the mechanism of K562 cells with GASC1 expression was able to stop proliferation at
279 the genetic level, we selected a range of key regular genes function as cell cycle effectors, such as
280 Rbl2, PRDM1, p21, p53, E2F4, lin9, and CDK2 [33,34]. Rbl2 (RB Transcriptional Corepressor Like

281 2) is a key regulator of entry into cell division [35], directly involved in heterochromatin formation
282 by stabilizing histone methylation, thus maintaining overall chromatin structure. In particular, Rbl2
283 acts as a transcription repressor by recruiting chromatin-modifying enzymes to promoters [35].
284 PRDM1 regulates the expression of genes involved in cell cycle. p21 is a cyclin-dependent kinase
285 (CDK) inhibitor that promotes cell cycle arrest, also acts as a gene downstream of p53 with linking
286 DNA damage to cell cycle arrest [33]. E2F4 is a key regulator to achieve and maintain cellular
287 quiescence by repressing cell cycle-regulated genes and plays an important role in the suppression
288 of proliferation-associated genes. Depletion of Lin9 results in an accumulation of cells in G2 and
289 M phases. CDK2 (Cyclin-dependent kinase 2) is a key cell cycle regulator, inactivating
290 phosphorylation of the RB1 and controlling both G1/S and G2/M transitions [34]. Based on the qPCR
291 results, we found that there is a remarkably increased transcription level of Rbl2, PRDM1, p21,
292 E2F4, lin9, CDK2 in the dox-induced GASC1 expression K562 cells than no dox cells (Fig. 6i).
293 p53 mRNA level was reduced markedly in the dox-induced GASC1 expression K562 cells. As
294 known, depletion of p53 in cells causes G1 arrest and apoptosis. Taken together, modulation of
295 GASC1 expression in leukemia cells leads to cell cycle arrest in the G0/G1 phase and shows
296 misshapen nuclei. Through regulating the activity of chromatin-modifying enzymes, that lead to
297 nuclear rupture and blebs, we sought to address a novel strategy to regulate cancer cell growth.
298

299 **Discussion**

300 The objective of this study was to investigate the manner in which both cellular and nuclear

301 size change during differentiation and how such changes might relevant to chromatin-modifying
302 enzymes. However, to date, there have not been many investigations of chromatin contribution to
303 nuclear morphology, although altered histone modifications and chromatin decompaction are
304 consistently present in both nuclei with abnormal morphology and nuclear blebs.

305 Lamins are fibrous proteins as well as nuclear structural proteins. Mouse ES cells express high
306 levels of A-type lamin during cell differentiation [36,37]. Forced expression of the progerin mutant
307 isoform of lamin A/C (LMAC) increases osteogenic differentiation and reduces adipogenic
308 differentiation [37]. Additionally, deregulation of lamin expression can lead to various cancer and be
309 used as diagnostic biomarkers. Lamin is a genetic reason for nuclear misshapen, however
310 epigenetic mechanism of nuclear shape change in cell fate determination is still obscure. Here, we
311 aim to understand whether activity alterations of chromatin-modifying enzymes affect nuclear
312 contour, and what mechanisms contribute to cellular identification of cell fate. We employed
313 histone-modifying enzyme inhibitors to get some clues of whether certain types of enzymes or all
314 histone-modifying enzymes are able to effect nuclear size alteration. We used stem cells such as
315 hESCs and NPCs to investigate the impact of histone-modifying enzyme inhibitors at the stage of
316 pluripotency and multipotency maintenance, which may have some distinctions. Also, we
317 investigated the impact of histone-modifying enzyme inhibitors on cancer cells such as leukemia
318 cells. We observed that there is enlarged nuclear size and misshapen nucleus via chromatin-
319 modifying enzyme inhibition. As known, heterochromatin appears larger, fewer, and decondensed
320 in ES cells, numerous and condensed in ES cell-derived neuronal progenitor cells, and appear

321 fewer but more compact in terminally differentiated neurons [38,39]. Additionally, cancer cells have
322 global alterations in chromatin organization, mostly a reduction in heterochromatin [40]. Therefore,
323 it suggested that the original histone states identify the specific type of cell, and impact the outcome
324 of histone-modifying enzymes inhibitors treatment.

325 In addition, when treated with histone-modifying enzyme inhibitors, the nuclear size was able
326 to alter, and the nuclear shape becomes aberrant. It demonstrated that chromatin state is a major
327 factor determining the morphology of the nucleus. The increase of nuclear blebbing in nucleus
328 which indicated that a consequence of increasing euchromatin or decreasing heterochromatin, and
329 decreasing nuclear rigidity. In addition, during dysregulation of histone by treatment of histone-
330 modifying enzyme inhibitors, some cells were unable to endure the stimulation and die, but some
331 cells with a misshapen nucleus survived. Is that the reconstructive chromatin provides certain
332 benefits for cell survival during chromatin-modifying enzyme dysregulation? After treatment of
333 histone-modifying enzyme inhibitors in NPCs, it was shown that the decreased expression of genes
334 who play a role in stem cell identification. We also observed the nuclear size become smaller and
335 smaller when cells were differentiated from hESCs to NPCs, then to iN cells. Simultaneously,
336 chromatin appears decondensed in ES cells, then appears more compact in differentiated neurons.
337 Collectively, it implies that the major function of chromatin-modifying enzyme is to determine cell
338 fate, nuclear size alteration is a phenomenon accompanied by the occurrence of cell lineage
339 commitment in normal cells.

340 As known, histone modifications correlate with ESC differentiation. Hundreds of promoters

341 of pluripotent genes gain their epigenetic marks, whereas many others lose it, during the transition
342 from ESC to NPCs, and from NPCs to differentiated neurons [41,42]. Through modulating chromatin-
343 modifying enzymes that are able to control a huge number of epigenetic marks on the promoters
344 of stem cell genes. Therefore, we ask for is that possible to modulate chromatin-modifying
345 enzymes to alter cancer cell fate. We selected three representative chromatin-modifying enzymes.
346 Unlike KDM4A-B, KDM4C (GASC1) is associated with chromatin during mitosis, and triggers
347 the demethylation of H3K9me3 mark [14]. Ectopic expression of GASC1 or other JMJD2 members
348 markedly decreases H3K9me3/me2 levels, increases H3K9me1 levels, delocalizes HP1
349 (heterochromatin protein 1), and reduces heterochromatin in vivo [19]. GASC1 is an Oct4 target in
350 mouse ES cells, and acts as a positive regulator of Nanog, also is preferentially expressed in
351 undifferentiated ES cells [12,43]. Depletion of GASC1 in ES cells induced differentiation with a
352 global increase in H3K9me3, confirming that the histone demethylase activity of GASC1 is linked
353 to the maintenance of pluripotency. The expression levels of GASC1 were also significantly related
354 to the grade of basal-like breast cancers which is the most aggressive type [18]. It suggested that
355 histone-modifying enzymes impact the cell fate of normal cells as well as cancer cells. To
356 investigate the impact of GASC1 in cancer cells, we manipulated GASC1 expression in a
357 commonly used leukemia cell line K562. We found that overexpression GASC1 impairs the cell
358 cycle process, deprives K562 cells proliferation capacity, and shows nuclear abnormalities. It
359 indicated that chromatin-modifying enzymes are associated with nuclear size determination and
360 cell fate decision of normal cells as well as cancer cells. Through modulating chromatin-modifying

361 enzymes activity which enables to deprive the aggressive proliferation capacity of cancer cells,
362 arrest cells in the cell cycle to die, and as a consequence, show nucleus misshapen.
363
364 **Methods**
365 **Cell culture and media.**
366 All cell types were maintained at 37°C in a humidified 5% (vol/vol) CO2 environment during
367 culture. H1 ES cells were obtained from WiCell Research Resources (WiCell, WI). ES cells were
368 maintained as feeder-free cells in mTeSR™1 medium (Stem Cell Technologies). Cells were
369 allowed to spread overnight prior to transduction. We used a doxycycline (dox)-inducible lentiviral
370 vector system to transduce empty vector plasmid as a control and GASC1, DNMT3A, KDM4A
371 into the H1 ES cells, separately. Selection was carried out for 7 days in mTeSR™1 medium with
372 50 μg/ml hygromycin.
373 **Generation of iN cells from human ES cells**
374 H1 human ESCs were dissociated using accutase and plated as single cells in mTeSR™1 medium
375 supplemented with ROCK inhibitor Y-27632 (10 μM, StemCell Technologies, Inc.) on matrigel to
376 a final density of 20,000-30,000 cells per cm^2. On the second day, attached cells were infected with
377 lentivirus for Ngn2-puro and rtTA expression. After 24 hr (day 0), transgene expression was
378 induced by replacing the medium with N2/B27 medium (DMEM/F12, N2 supplement (Life
379 Technologies), B27 supplement (Life Technologies), 10 μg/ml insulin (Life Technologies)), and
380 2 μg/ml Doxycycline. Selection was carried out for 14 days (day 1 to day 14) in N2/B27 medium

381 with 2 μg/ml puromycin. From day 2, induced neuronal cells were maintained in N2/B27 medium
382 and changed medium every 2 days.

383 **hESCs differentiate to neural progenitor cells**

384 Growing hESCs in mTeSR media on matrigel coated dish until confluent, then enzymatically
385 passage with accutase, resuspend in Neurobasal-A medium, DMEM/F12, 1% N2, 1% B27 and
386 insulin media, with Y-27632, a specific inhibitor of Rho kinase (ROCK) activity, cultured in the
387 same size of the dish without matrigel coated. Overnight, colonies will form floating spherical
388 clusters termed "embryoid bodies" (EBs). Wait until the EB size grows to 200～400 μm, gently
389 move it to matrigel coated dish. The next day, it will attach to the bottom. Changing medium with
390 N2/B27 media supplemented with dual SMAD inhibitors (0.1 μM LDN193189 and 10 μM
391 SB431542). Feed EBs every second day with N2/B27 media supplemented with 0.1 μM
392 LDN193189 and 10 μM SB431542. After several days, the neural rosettes begin to appear,
393 characterized as round clusters of neuroepithelial cells with apicobasal polarity. Staining Sox1 to
394 indicate the neural progenitor cells.

395 **Virus generation**

396 Lentiviruses were produced as described [44] in HEK293T cells (ATCC, VA) by co-transfection with
397 three helper plasmids (pRSV-REV, pMDLg/pRRE and vesicular stomatitis virus G protein
398 expression vector) (12 μg of lentiviral vector DNA and 6 μg of each of the helper plasmid DNA
399 per 75 cm^2 culture area) using calcium phosphate [8]. Lentiviruses were harvested with the medium
400 24 and 46 hr after transfection. Viral supernatant was filtered through a 0.45 μm filter, pelleted by

401 centrifugation (21,000 × g for 2 hours), resuspended in DMEM, aliquoted, and snap-frozen in
402 liquid N_2. Only virus preparations with >90% infection efficiency as assessed by EGFP expression
403 or puromycin resistance were used for experiments.

404 **Lentiviral infections**

405 Complementary DNAs for candidate genes were cloned into doxycycline-inducible lentiviral
406 vectors, as described previously [45]. Lentiviral production and cell infection was performed as
407 described previously [46]. Cells were infected with concentrated lentivirus and treated with
408 doxycycline (2 mg/ul) 16-24 h later.

409 **Immunofluorescence**

410 Cultured iN cells were fixed in 4% paraformaldehyde in PBS for 15 min at room temperature,
411 washed three times with PBS, and incubated in 0.2% Triton X-100 in PBS for 10 min at room
412 temperature. Cells were blocked in PBS containing 10% BSA for 3 hours at 4°C. Primary
413 antibodies were applied overnight. Cells were washed in PBS three times. Secondary antibodies
414 were applied for 3 hours, washed. 300 nM DAPI staining for indication of nucleus. Mount.

415 **Antibody**

416 The following primary antibodies with indicated dilution in blocking buffer were used: Rabbit
417 anti-Tuj1 (Covance, BioLegend, MRB-435P, 1:1,000), Mouse anti-Tuj1 (Covance, BioLegend,
418 MMS-435P, 1:1,000), Rabbit anti-human Sox1 (Millipore, AB15766), Goat anti-Sox2 (Santa Cruz,
419 1:200). After staining with corresponding secondary antibodies in PBS plus 1% BSA, coverslips
420 were washed four times with PBS, each for 10 min, mounted with the mounting medium onto glass

421 slides, and examined under Olympus FluoView FV1000.

422 **Inhibitors of chromatin-modifying enzymes**

423 Purchase from tocris. GSK J1 (Cat. No. 4593), (R)-2-Hydroxyglutaric acid disodium salt (R2-HG,
424 Cat. No. 6124), GSK-LSD 1 dihydrochloride (Cat. No. 5361), IOX 1 (Cat. No. 4464/10), JIB04
425 (Cat. No. 4972/10), NSC636819 (Cat. No. 5287/10), PBIT (Cat. No. 5930), C646 (Cat. No.
426 4200/10), 5-azacytidine (5-Aza, Cat. No. 3842).

427 **qRT-PCR**

428 RNA was isolated through standard methods following manufacturer's instructions (QIAGEN),
429 and reverse transcribed with Superscript III (Life Technology). qRT-PCR was performed with Fast
430 Start universal SYBR green master mix (Roche) along with gene specific primers on a 7900HT
431 real-time PCR machine (Applied Biosystems). Statistical significance was determined by Students
432 t test based on triplicated experiments.

433 **Flow cytometry**

434 Flow cytometry was used to sort live cells by their size and cell cycle phase. The cells were
435 harvested by trypsinization, then stained with 20 μM Hoechst 33342 which is a DNA dye in PBS
436 for 15 minutes at 37°C and then sorted on a BD FACSAria flow cytometer. DNA content was used
437 to determine cell cycle phase, and the forward scatter area parameter was used as a readout for cell
438 size. Flow cytometry data was prepared for presentation using FlowJo2.

439 **Coulter counter**

440 Coulter counter is an apparatus for counting and sizing particles suspended in electrolytes. We use

441 the Z2 Coulter counter (Beckman). After collect the cells by trypsinization and spin down on
442 centrifuge, then resuspend in PBS, it is ready to run them through the counter (no staining needed).
443 Turn on the coulter counter and setup calibration as user's manual. Add your cell samples in
444 accuvette and gently mix then enter the accuvette on counting platform. Then, setting up the
445 aperture diameter, current Kd, and lines for selecting units and set the upper and lower size
446 expected particle sizes. Run the cell samples. Export the data for analysis later. The size
447 distribution of the sorted cells was determined using the Z2 Coulter Counter and Multisizer III
448 software (Beckman Coulter).

449 **Statistical Tests**

450 Microsoft Excel was used for data analysis. Experiments were performed in a blinded fashion; i.e.,
451 the experimenter was unaware of the genotype of the samples being studied. Cumulative plots
452 were generated from parameters collected from individual cells under similar experimental
453 conditions. Average data are presented as bar graphs indicating means ± SD. Statistical
454 comparisons between bar graphs were made using the unpaired, one-tail, Student t test (*$P < 0.05$,
455 **$P < 0.01$, and ***$P < 0.001$, all versus control).

Acknowledgements

We would like to thank all our laboratory members and collaborators for their comments and dedicated work that have greatly contributed to the ideas presented here. L.M. was supported by the California Institute of Regenerative Medicine (CIRM). This study was supported by the Howard Hughes Medical Institute Faculty Scholar Award (M.W.), and the NIH R01 grant.

Author Contributions

L.M., E.Z. and M.W. conceived and designed the study; L.M., E.Z., planned and performed the experiments; L.M., E.Z., performed FACS and Coulter counter; J.S. and M.W. provided critical advice on experimental designs and data interpretations; K.S. and G.N. provided experimental material; K.S. revised the manuscript and thank for helpful comments on the manuscript. L.M. wrote the manuscript.

Declaration of Interests

The authors declare no conflicts of interest in the presented study.

471 **FIGURE LEGENDS**

472 **Fig. 1 Nuclear size is associated with cell fate decision and chromatin-modifying enzyme**
473 **activity.**

474 **a,** Immunofluorescence staining cell nucleus of hESCs, hESC-derived NPCs, hESC-derived iN
475 cells by DAPI (blue).

476 **b,** Measurements of cell nucleus size of hESCs, hESC-derived NPCs, hESC-derived iN cells by
477 DAPI staining. ***$p < 0.001$. White scale bars= 50 μm.

478 **c,** Brightfield and fluorescent images of hESCs and hESC-derived NPCs immunofluorescence
479 staining for H3K9me3 (red) and DAPI (blue).

480 **d,** Measurements of nuclear size after hESCs treated with histone demethylase inhibitors (GSK J1,
481 (R)-2-Hydroxyglutaric acid disodium salt, GSK-LSD1, IOX1, JIB04, NSC636819, PBIT), DNA
482 methyltransferase inhibitor (5-Azacytidine), and histone acetyltransferase inhibitor (C646) by
483 DAPI staining. Statistically significant differences are marked with asterisks. *$P < 0.05$, **$p <$
484 0.01, ***$p < 0.001$.

485 **e,** Measurements of nuclear size by DAPI staining after hESC-derived NPCs treated with
486 chromatin-modifying enzymes inhibitors.

487 **f,** Measurements of nuclear size by DAPI staining after hESC-derived iN cells treated with DMSO
488 as control and 5-Aza.

489 **g,** Representative immunocytochemistry images of hESCs stained with DAPI. hESCs treated with
490 DMSO as control and 5-Aza. It was shown that the bigger nuclei occurred at 5-Aza treatment. The

491 images were taken at 40× on a confocal microscope. Red scale bars= 20 μm.

492

493 **Fig. 2 Inhibition of chromatin-modifying enzyme enlarges hESCs nuclear size.**

494 **a, b, c,** Using flow cytometry assay to measure cell size and nuclear size after chromatin-modifying

495 enzymes inhibitors treatment of hESCs for 7 days. FSC-A indicates cell size. Hoechst-W (width)

496 indicates nuclear size.

497 **d, e,** After inhibitors treatment, measuring cell size and nuclear size by flow cytometry. FSC-A

498 indicates cell size. Hoechst-W (width) indicates nuclear size. Each group normalizes to DMSO

499 control. *P < 0.05.

500 **f,** The cell volume of hESCs was measured with coulter counter after inhibitors treatment for 6

501 days. The curve was calculated from the coulter counter measurements of asynchronous size

502 distribution. FL (Femtoliter). *P < 0.05.

503

504 **Fig. 3 Inhibition of chromatin-modifying enzyme effects nuclear size and cell identification**

505 **of NPCs.**

506 **a,** Fluorescent images of hESC-derived NPCs immunofluorescence staining for Sox1 (green), PI

507 (red), and DAPI (blue) after treatment with inhibitors of chromatin-modifying enzymes. White

508 scale bars= 50 μm.

509 **b,** Histogram showing the cell size of hESC-derived NPCs measured by coulter counter after

510 inhibitors treatment for 9 days compared with DMSO control. Two-tailed t-test, Mean ± SD. *P <

511 0.05.

512

513 **Fig. 4 Inhibition of chromatin-modifying enzyme effects leukemia cell nuclear architecture.**

514 **a, b, c,** Using flow cytometry to measure cell size and nuclear size of K562 leukemia cells after

515 inhibitors treatment for 5 days. FSC-A indicates cell size. Hoechst-W (width) indicates nuclear

516 size.

517 **d,** Representative images of DAPI staining for K562 cells treated with DMSO as control and 5-

518 Aza, IOX1, GSK-LSD1, and JIB04. It was shown that the bigger size and twisted shape of nuclei

519 in inhibitors treatment. The images were taken at 40× on a confocal microscope. White scale bars=

520 25 μm.

521 **e,** Measurements of the nuclear size using DAPI staining and fluorescence microscopy after K562

522 cells treated with inhibitors of chromatin-modifying enzymes. Two-tailed t-test, Mean ± SD. **p

523 < 0.01, ***p < 0.001.

524 **f,** Measuring cell size and nuclear size of K562 cells through flow cytometry, DAPI staining, and

525 coulter counter after inhibitors treatment for 7 days. Using flow cytometry to measure cell size and

526 nuclear size. Measuring nuclear size after DAPI staining by confocal microscope. Coulter counter

527 measures cell size. The average values for each treatment were normalized to DMSO control. ***p

528 < 0.001.

529

530 **Fig. 5 Upregulated GASC1 impairs differentiation from hESCs to iN cells.**

531 **a,** Brightfield and fluorescent images of the hESC-derived iN cells with wt, dox-induced
532 overexpression of GASC1, DNMT3A, and KDM4A stained for the pluripotent marker Sox2
533 (green), the neural cells marker Tuj1 (red), and nucleus staining DAPI (blue) after 14 days of iN
534 cells differentiation.
535 **b,** Neurite length of the hESC-derived iN cells was measured at 14 days of iN cells differentiation.
536 p-values were calculated by unpaired t-test, error bars represent standard deviation, * $p < 0.05$, ***
537 $p < 0.001$.
538
539 **Fig. 6 GASC1 promotes aberrant nuclear structure and cell cycle arrest of leukemia cells.**
540 **a,** Brightfield and fluorescent images show that K562 leukemia cells differentiate to iN cells with
541 Ngn2 overexpression after 14 days differentiation and stain with the neuronal marker Tuj1 (red).
542 The yellow arrows indicate the cells of morphological changes.
543 **b, c,** Brightfield images of the K562 leukemia cells with induced expression of GASC1 with or
544 without doxycycline (dox). The no dox-induced GASC1 overexpression K562 cells show spherical
545 morphology, same as normal cells. The dox-induced GASC1 overexpression K562 cells show
546 morphology change from spherical to twisted shape and nuclear blebs. The red arrow indicates the
547 cells with twisted shapes. White scale bars= 25 μm.
548 **d, e,** Fluorescent images by DAPI staining demonstrate that the dox-induced GASC1
549 overexpression K562 cells show the twisted nuclear shape and bigger nuclei compared with the no
550 dox-induced GASC1 overexpression K562 cells. The red arrow indicates the enlarged and twisted

551 nucleus.

552 **f, g,** Flow cytometric analysis of K562 cells were double-stained with BrdU and PI. The dox-

553 induced GASC1 overexpression K562 cells proliferate significantly slower than the no dox-

554 induced GASC1 overexpression K562 cells by Brdu assay.

555 **h,** Cell number counting after induction by dox for 7 days. The cell number is decreased in dox-

556 induced GASC1 overexpression K562 cells than no dox-induced GASC1 overexpression K562

557 cells. ***$p < 0.001$. n=3.

558 **i,** The genes play a role in cell-cycle arrest detected by qPCR in the dox-induced GASC1

559 overexpression K562 cells and no dox-induced GASC1 overexpression K562 cells. Unpaired two-

560 tailed Student t-test. Data are mean ± SD. $p < 0.001$.

561 **REFERENCES**

562 1 Tamashunas, A. C. *et al.* High-throughput gene screen reveals modulators of nuclear shape.
563 *Mol Biol Cell* **31**, 1392-1402 (2020).

564 2 McBeath, R., Pirone, D. M., Nelson, C. M., Bhadriraju, K. & Chen, C. S. Cell shape,
565 cytoskeletal tension, and RhoA regulate stem cell lineage commitment. *Dev Cell* **6**, 483-
566 495 (2004).

567 3 Bartova, E., Krejci, J., Harnicarova, A. & Kozubek, S. Differentiation of human embryonic
568 stem cells induces condensation of chromosome territories and formation of
569 heterochromatin protein 1 foci. *Differentiation* **76**, 24-32 (2008).

570 4 Pajerowski, J. D., Dahl, K. N., Zhong, F. L., Sammak, P. J. & Discher, D. E. Physical
571 plasticity of the nucleus in stem cell differentiation. *Proc Natl Acad Sci U S A* **104**, 15619-
572 15624 (2007).

573 5 Tzur, A., Kafri, R., LeBleu, V. S., Lahav, G. & Kirschner, M. W. Cell growth and size
574 homeostasis in proliferating animal cells. *Science* **325**, 167-171 (2009).

575 6 Tzur, A., Moore, J. K., Jorgensen, P., Shapiro, H. M. & Kirschner, M. W. Optimizing optical
576 flow cytometry for cell volume-based sorting and analysis. *PLoS One* **6**, e16053 (2011).

577 7 Gregg, E. C. & Steidley, K. D. Electrical counting and sizing of mammalian cells in
578 suspension. *Biophys J* **5**, 393-405 (1965).

579 8 Pang, Z. P., Cao, P., Xu, W. & Sudhof, T. C. Calmodulin controls synaptic strength via
580 presynaptic activation of calmodulin kinase II. *J Neurosci* **30**, 4132-4142 (2010).

581 9 Shen, H., Xu, W. & Lan, F. Histone lysine demethylases in mammalian embryonic
582 development. *Exp Mol Med* **49**, e325 (2017).
583 10 He, J. *et al.* Kdm2b maintains murine embryonic stem cell status by recruiting PRC1
584 complex to CpG islands of developmental genes. *Nat Cell Biol* **15**, 373-384 (2013).
585 11 Pereira, J. D. *et al.* Ezh2, the histone methyltransferase of PRC2, regulates the balance
586 between self-renewal and differentiation in the cerebral cortex. *Proc Natl Acad Sci U S A*
587 **107**, 15957-15962 (2010).
588 12 Loh, Y. H., Zhang, W., Chen, X., George, J. & Ng, H. H. Jmjd1a and Jmjd2c histone H3
589 Lys 9 demethylases regulate self-renewal in embryonic stem cells. *Genes Dev* **21**, 2545-
590 2557 (2007).
591 13 Kottakis, F. *et al.* NDY1/KDM2B functions as a master regulator of polycomb complexes
592 and controls self-renewal of breast cancer stem cells. *Cancer Res* **74**, 3935-3946 (2014).
593 14 Kupershmit, I., Khoury-Haddad, H., Awwad, S. W., Guttmann-Raviv, N. & Ayoub, N.
594 KDM4C (GASC1) lysine demethylase is associated with mitotic chromatin and regulates
595 chromosome segregation during mitosis. *Nucleic Acids Res* **42**, 6168-6182 (2014).
596 15 Yang, Z. Q. *et al.* Identification of a novel gene, GASC1, within an amplicon at 9p23-24
597 frequently detected in esophageal cancer cell lines. *Cancer Res* **60**, 4735-4739 (2000).
598 16 Northcott, P. A. *et al.* Multiple recurrent genetic events converge on control of histone
599 lysine methylation in medulloblastoma. *Nat Genet* **41**, 465-472 (2009).
600 17 Xiao, Z. *et al.* GASC1 promotes glioma progression by enhancing NOTCH1 signaling.

601 *Mol Med Rep* **23** (2021).

602 18 Liu, G. *et al.* Genomic amplification and oncogenic properties of the GASC1 histone
603 demethylase gene in breast cancer. *Oncogene* **28**, 4491-4500 (2009).

604 19 Cloos, P. A. *et al.* The putative oncogene GASC1 demethylates tri- and dimethylated lysine
605 9 on histone H3. *Nature* **442**, 307-311 (2006).

606 20 Wu, L. *et al.* Histone Demethylases KDM4A and KDM4C Regulate Differentiation of
607 Embryonic Stem Cells to Endothelial Cells. *Stem Cell Reports* **5**, 10-21 (2015).

608 21 Richly, H., Aloia, L. & Di Croce, L. Roles of the Polycomb group proteins in stem cells
609 and cancer. *Cell Death Dis* **2**, e204 (2011).

610 22 Heo, S. J. *et al.* Differentiation alters stem cell nuclear architecture, mechanics, and
611 mechano-sensitivity. *Elife* **5** (2016).

612 23 Chambers, S. M. *et al.* Highly efficient neural conversion of human ES and iPS cells by
613 dual inhibition of SMAD signaling. *Nat Biotechnol* **27**, 275-280 (2009).

614 24 Zhang, Y. *et al.* Rapid single-step induction of functional neurons from human pluripotent
615 stem cells. *Neuron* **78**, 785-798 (2013).

616 25 Volpe, T. A. *et al.* Regulation of heterochromatic silencing and histone H3 lysine-9
617 methylation by RNAi. *Science* **297**, 1833-1837 (2002).

618 26 Lee, K. K. & Workman, J. L. Histone acetyltransferase complexes: one size doesn't fit all.
619 *Nat Rev Mol Cell Biol* **8**, 284-295 (2007).

620 27 Stephens, A. D. *et al.* Chromatin histone modifications and rigidity affect nuclear

621 morphology independent of lamins. *Mol Biol Cell* **29**, 220-233 (2018).

622 28 Fischer, E. G. Nuclear Morphology and the Biology of Cancer Cells. *Acta Cytol* **64**, 511-
623 519 (2020).

624 29 Papanicolaou, G. N. & Traut, H. F. The diagnostic value of vaginal smears in carcinoma of
625 the uterus. 1941. *Arch Pathol Lab Med* **121**, 211-224 (1997).

626 30 Sullivan, T. *et al.* Loss of A-type lamin expression compromises nuclear envelope integrity
627 leading to muscular dystrophy. *J Cell Biol* **147**, 913-920 (1999).

628 31 Dang, L. *et al.* Cancer-associated IDH1 mutations produce 2-hydroxyglutarate. *Nature* **462**,
629 739-744 (2009).

630 32 Lu, C. *et al.* IDH mutation impairs histone demethylation and results in a block to cell
631 differentiation. *Nature* **483**, 474-478 (2012).

632 33 Koivomagi, M., Swaffer, M. P., Turner, J. J., Marinov, G. & Skotheim, J. M. G1 cyclin-
633 Cdk promotes cell cycle entry through localized phosphorylation of RNA polymerase II.
634 *Science* **374**, 347-351 (2021).

635 34 Coffman, J. A. Cell cycle development. *Dev Cell* **6**, 321-327 (2004).

636 35 Litovchick, L. *et al.* Evolutionarily conserved multisubunit RBL2/p130 and E2F4 protein
637 complex represses human cell cycle-dependent genes in quiescence. *Mol Cell* **26**, 539-551
638 (2007).

639 36 Galiova, G., Bartova, E., Raska, I., Krejci, J. & Kozubek, S. Chromatin changes induced
640 by lamin A/C deficiency and the histone deacetylase inhibitor trichostatin A. *Eur J Cell*

641 *Biol* **87**, 291-303 (2008).

642 37 Scaffidi, P. & Misteli, T. Lamin A-dependent misregulation of adult stem cells associated
643 with accelerated ageing. *Nat Cell Biol* **10**, 452-459 (2008).

644 38 Meshorer, E. *et al.* Hyperdynamic plasticity of chromatin proteins in pluripotent embryonic
645 stem cells. *Dev Cell* **10**, 105-116 (2006).

646 39 Meshorer, E. & Misteli, T. Chromatin in pluripotent embryonic stem cells and
647 differentiation. *Nat Rev Mol Cell Biol* **7**, 540-546 (2006).

648 40 Gurrion, C., Uriostegui, M. & Zurita, M. Heterochromatin Reduction Correlates with the
649 Increase of the KDM4B and KDM6A Demethylases and the Expression of Pericentromeric
650 DNA during the Acquisition of a Transformed Phenotype. *J Cancer* **8**, 2866-2875 (2017).

651 41 Bernstein, B. E. *et al.* A bivalent chromatin structure marks key developmental genes in
652 embryonic stem cells. *Cell* **125**, 315-326 (2006).

653 42 Mikkelsen, T. S. *et al.* Genome-wide maps of chromatin state in pluripotent and lineage-
654 committed cells. *Nature* **448**, 553-560 (2007).

655 43 Katoh, Y. & Katoh, M. Comparative integromics on JMJD2A, JMJD2B and JMJD2C:
656 preferential expression of JMJD2C in undifferentiated ES cells. *Int J Mol Med* **20**, 269-273
657 (2007).

658 44 Brambrink, T. *et al.* Sequential expression of pluripotency markers during direct
659 reprogramming of mouse somatic cells. *Cell Stem Cell* **2**, 151-159 (2008).

660 45 Stadtfeld, M., Maherali, N., Breault, D. T. & Hochedlinger, K. Defining molecular

661 cornerstones during fibroblast to iPS cell reprogramming in mouse. *Cell Stem Cell* **2**, 230-
662 240 (2008).
663 46 Chen, C. & Okayama, H. High-efficiency transformation of mammalian cells by plasmid
664 DNA. *Mol Cell Biol* **7**, 2745-2752 (1987).
665

Figure 1

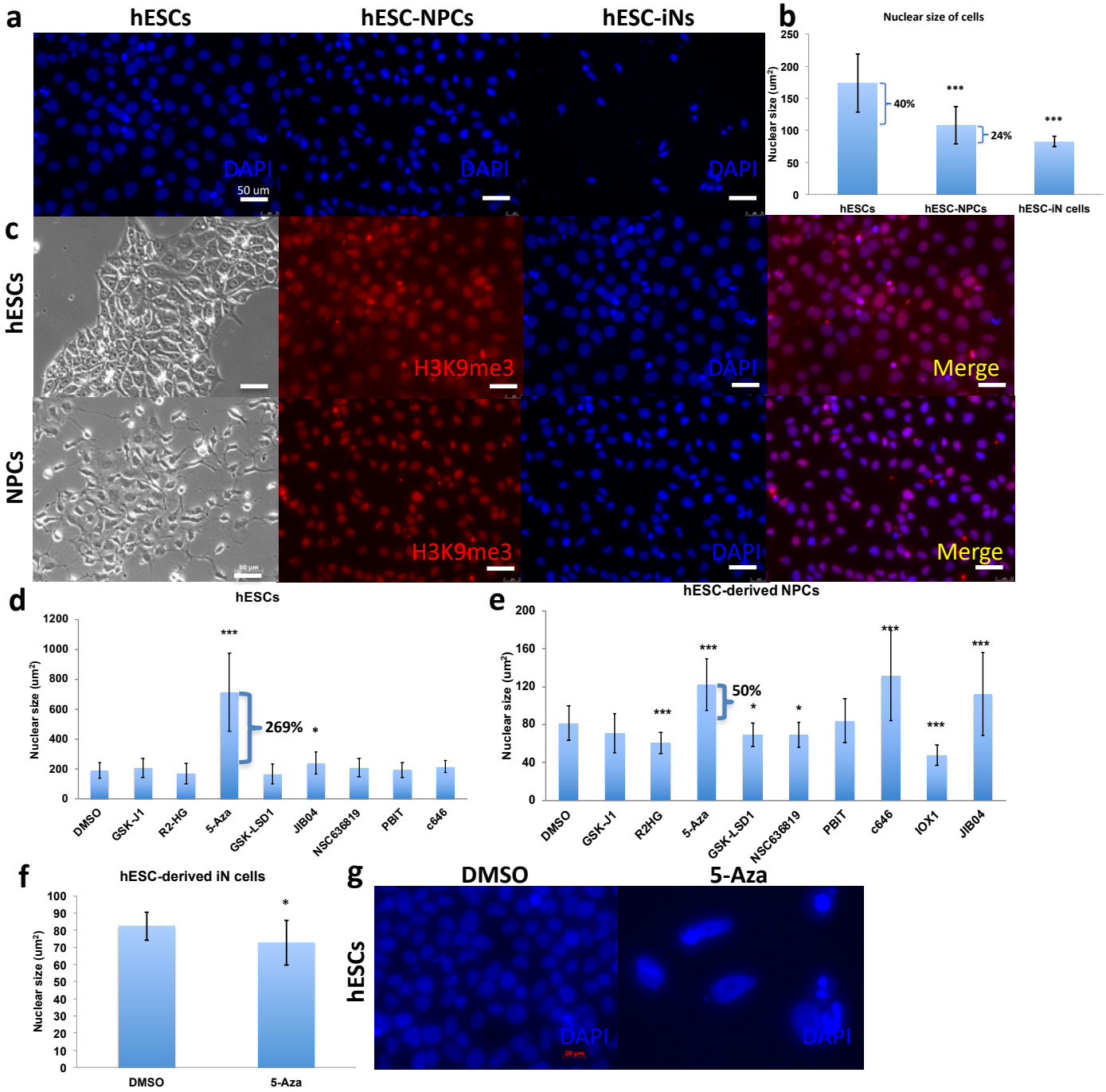
a
hESCs
hESC-NPCs
hESC-iNs
DAPI
50 um
b
Nuclear size of cells
Nuclear size (um²)
40%
24%
***
hESCs
hESC-NPCs
hESC-iN cells
c
hESCs
NPCs
H3K9me3
DAPI
Merge
d
hESCs
269%
DMSO
GSK-J1
R2-HG
5-Aza
GSK-LSD1
JIB04
NSC636819
PBIT
c646
e
hESC-derived NPCs
50%
R2HG
IOX1
f
hESC-derived iN cells
DMSO
5-Aza
g
DMSO
5-Aza
hESCs

Figure 2

a

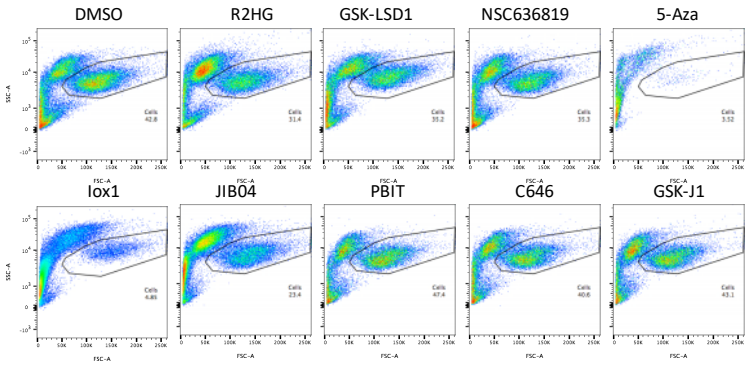

b

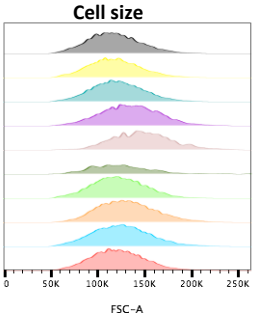

Sample Name	Median : FSC-A	Mean : FSC-A
11-hESC-GSK-J1	115520	117268
10-hESC-C646	116416	117796
9-hESC-PBIT	120064	121334
8-hESC-JIB04	133760	134471
7-hESC-Iox1	146176	147181
6-hESC-5-Aza	121216	125199
5-hESC-NSC636819	120768	121848
4-hESC-GSK-LSD1	129024	130928
3-hESC-R2HG	124160	125379
1-hESC-DMSO	120192	121612

c

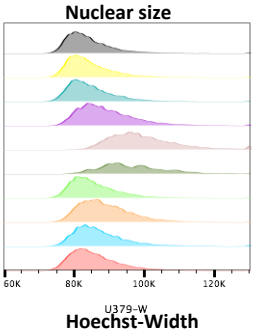

Sample Name	Median : U379-W	Mean : U379-W
11-hESC-GSK-J1	82661	84271
10-hESC-C646	82866	84521
9-hESC-PBIT	83413	84970
8-hESC-JIB04	87617	89308
7-hESC-Iox1	97854	99517
6-hESC-5-Aza	95120	96788
5-hESC-NSC636819	84199	85738
4-hESC-GSK-LSD1	87566	88907
3-hESC-R2HG	85789	87515
1-hESC-DMSO	84336	85731

d

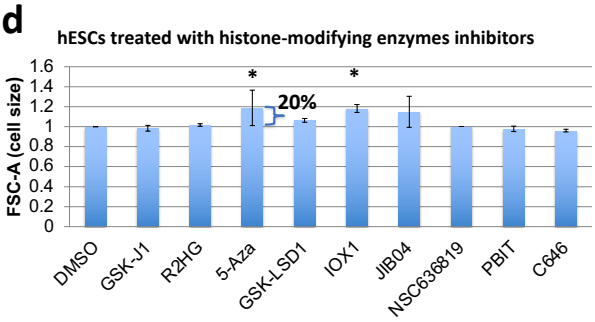

e

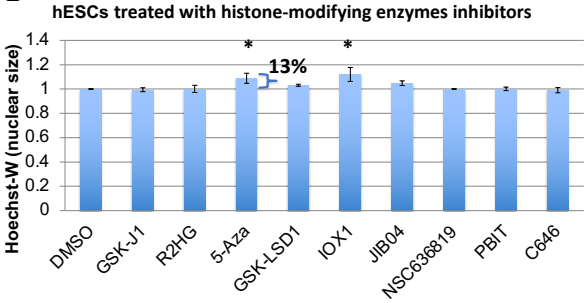

f

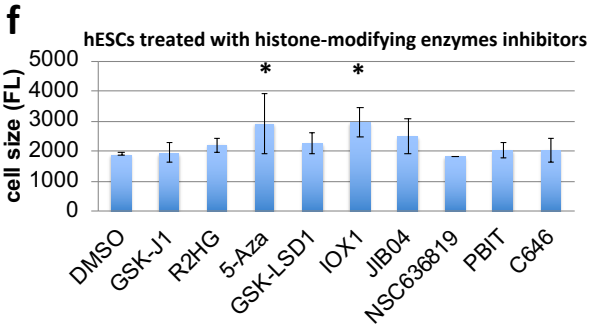

f

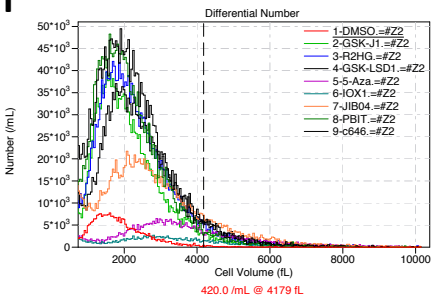

	Amount	MCV	S.D.
1-DMSO.=#Z2	267.1e3	1,932	793
2-GSK-J1.=#Z2	1.571e6	2,171	935
3-R2HG.=#Z2	1.900e6	2,356	1,061
4-GSK-LSD1.=#Z2	1.737e6	2,505	1,085
5-5-Aza.=#Z2	435.8e3	3,634	1,564
6-IOX1.=#Z2	174.7e3	3,287	1,457
7-JIB04.=#Z2	1.272e6	2,898	1,378
8-PBIT.=#Z2	2.031e6	2,191	953
9-c646.=#Z2	2.306e6	2,322	1,045

Figure 3

a

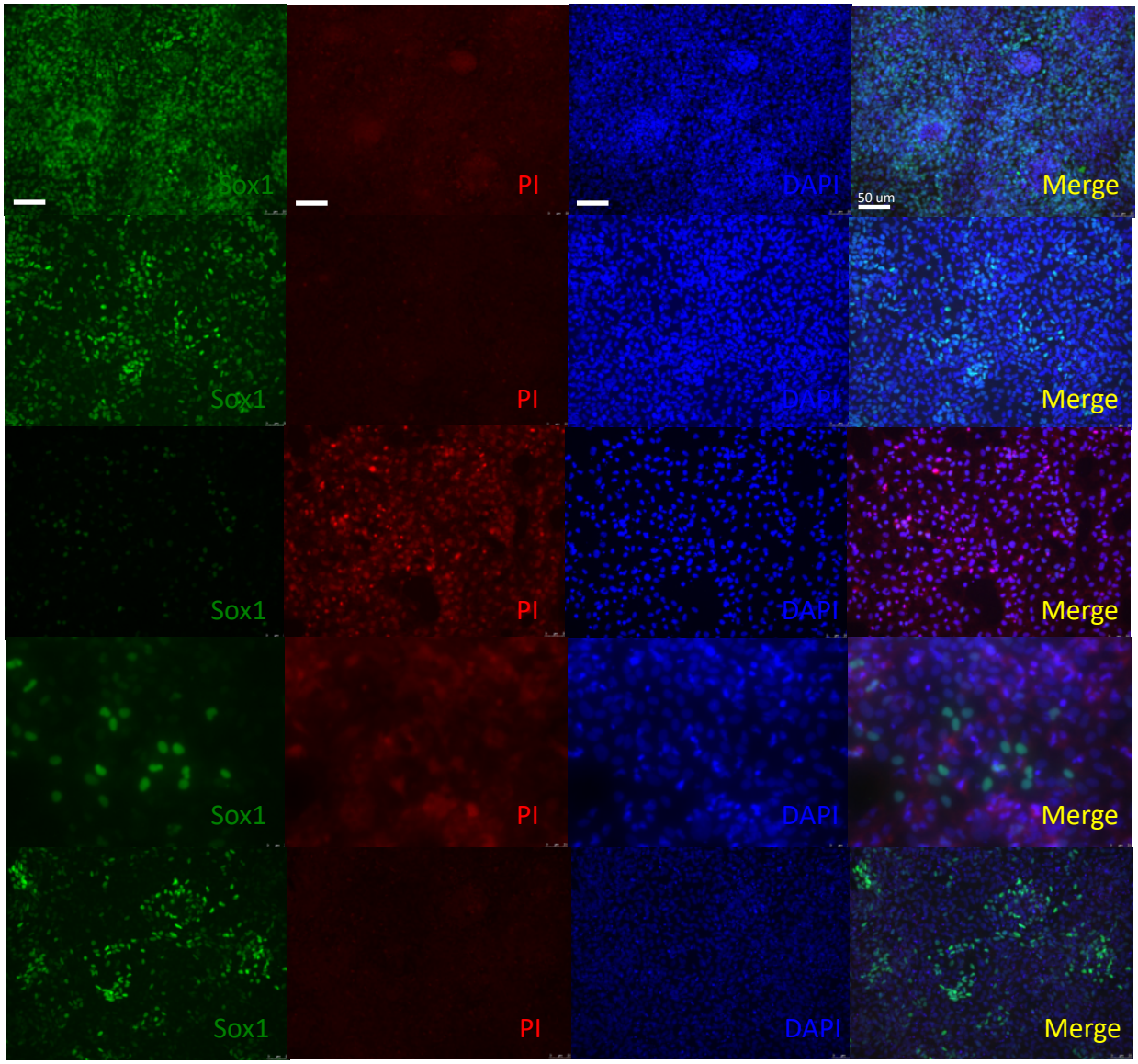

b

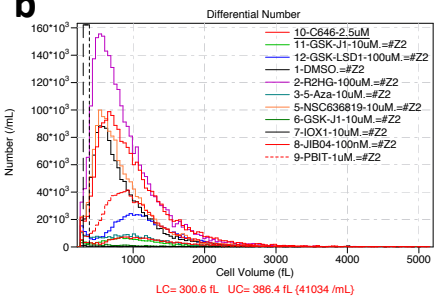

	Amount	MCV	S.D
10-C646-2.5uM	1.930e6	1,010	571
11-GSK-J1-10uM.=#Z2	157.2e3	1,125	711
12-GSK-LSD1-100uM.	569.6e3	1,140	501
1-DMSO.=#Z2	1.315e6	835	460
2-R2HG-100uM.=#Z2	2.632e6	872	474
3-5-Aza-10uM.=#Z2	249.7e3	1,048	640
5-NSC636819-10uM.=	1.514e6	860	474
6-GSK-J1-10uM.=#Z2	41,874	1,070	809
7-IOX1-10uM.=#Z2	14,826	1,170	913
8-JIB04-100nM.=#Z2	196.9e3	1,285	848
9-PBIT-1uM.=#Z2	843.1e3	1,065	538

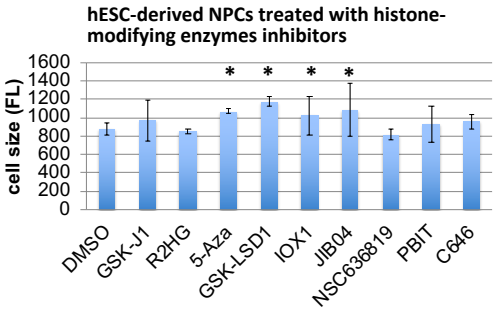

Figure 4

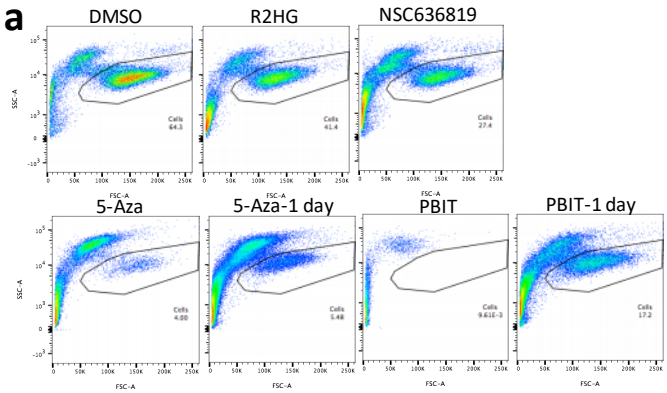

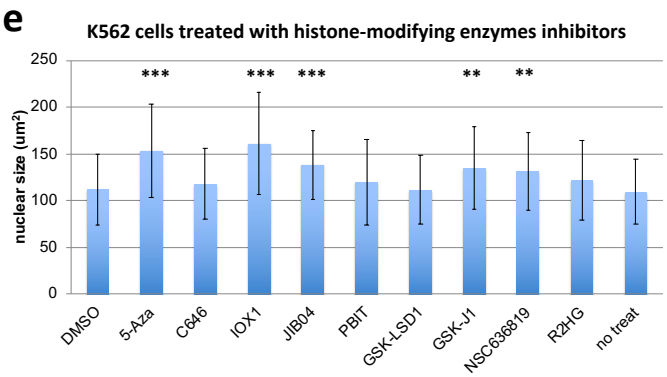

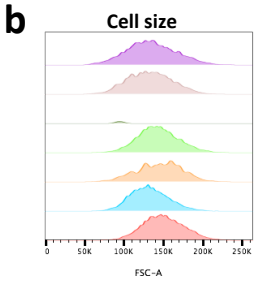

	Sample Name	Median : FSC-A	Mean : FSC-A
	K562-12-PBIT-1day	132864	134266
	K562-11-5-Aza-1day	131968	132353
	K562-9-PBIT	93952	93952
	K562-8-MSC636819	141440	142764
	K562-4-5-Aza	145536	144071
	K562-3-R2HG	130496	132004
	K562-1-DMSO	148224	149426

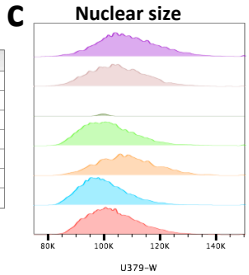

	Sample Name	Median : U379-W	Mean : U379-W
	K562-12-PBIT-1day	107611	108680
	K562-11-5-Aza-1day	104279	104916
	K562-9-PBIT	99573	99573
	K562-8-MSC636819	100891	102150
	K562-4-5-Aza	107648	108222
	K562-3-R2HG	99023	100162
	K562-1-DMSO	102319	103442

Hoechst-Width

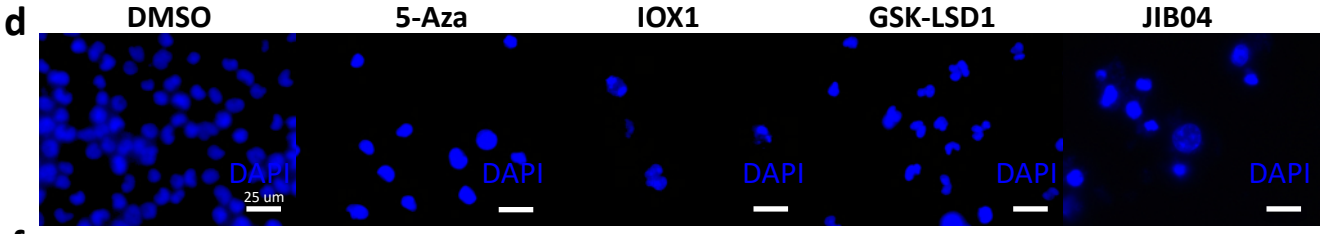

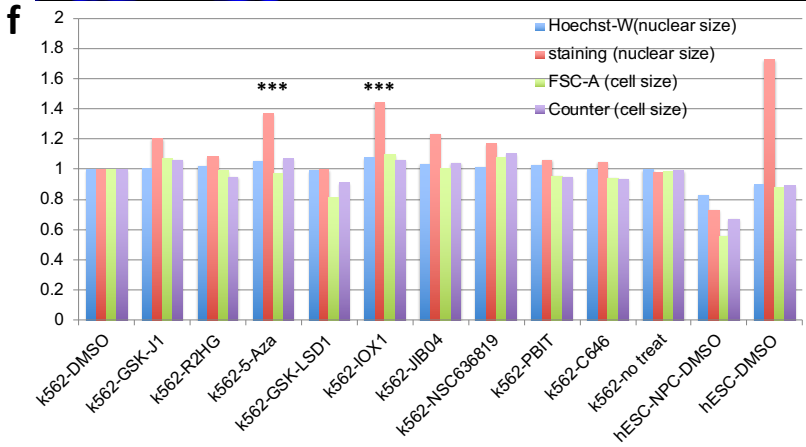

Figure 5

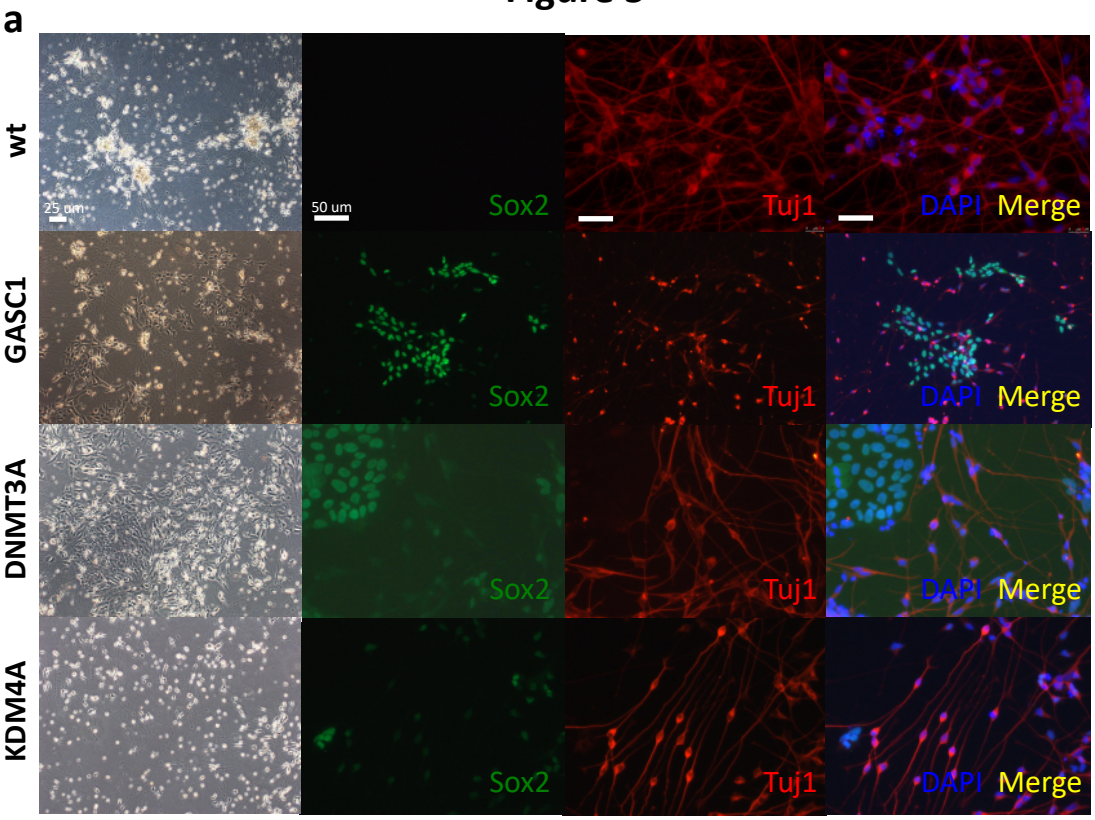
a
wt
GASC1
DNMT3A
KDM4A
25 um
50 um
Sox2
Tuj1
DAPI
Merge

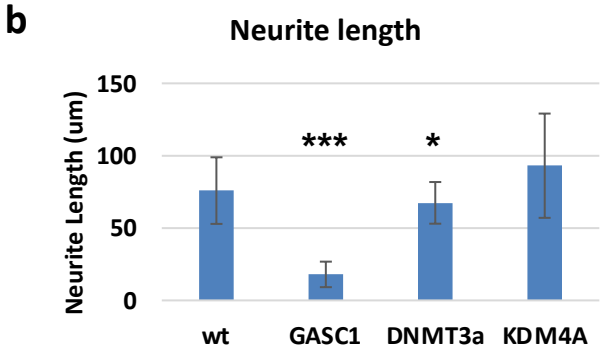
b
Neurite length
Neurite Length (um)
150
100
50
0
***
*
wt
GASC1
DNMT3a
KDM4A

Figure 6

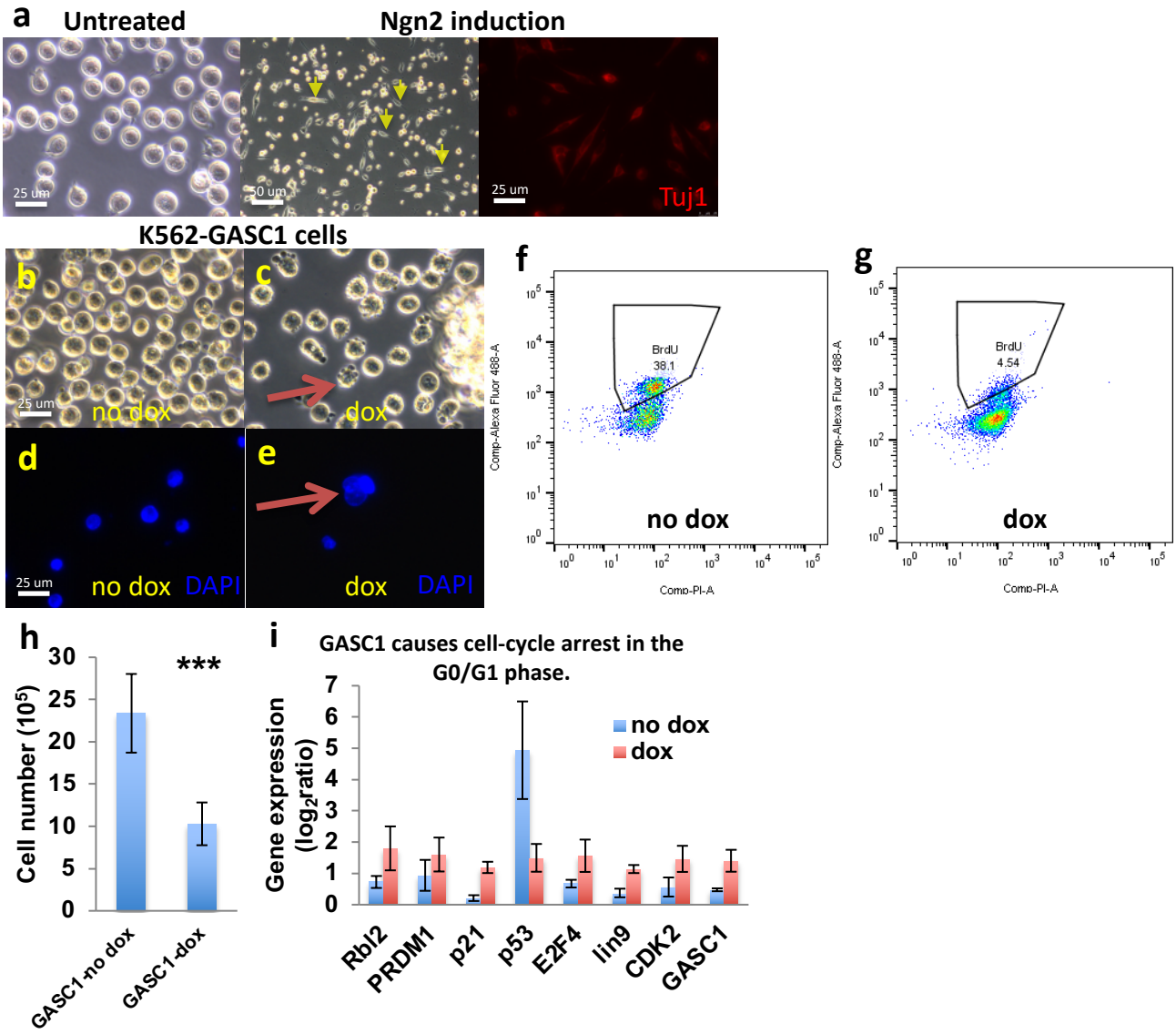
a
Untreated
Ngn2 induction
25 um
50 um
25 um
Tuj1
K562-GASC1 cells
b
c
25 um
no dox
dox
d
e
25 um
no dox
DAPI
dox
DAPI
f
g
BrdU
38.1
no dox
BrdU
4.54
dox
Comp-Alexa Fluor 488-A
Comp-PI-A
h
Cell number (10^5)
***
GASC1-no dox
GASC1-dox
i
GASC1 causes cell-cycle arrest in the G0/G1 phase.
Gene expression (log_2ratio)
no dox
dox
Rbl2
PRDM1
p21
p53
E2F4
lin9
CDK2
GASC1